ADVANCED MATERIALS
www.advmat.de

3.88% Efficient Tin Sulfide Solar Cells using Congruent Thermal Evaporation

Vera Steinmann, R. Jaramillo, Katy Hartman, Rupak Chakraborty, Riley E. Brandt, Jeremy R. Poindexter, Yun Seog Lee, Leizhi Sun, Alexander Polizzotti, Helen Hejin Park, Roy G. Gordon, and Tonio Buonassisi*

The demand for low-cost and scalable renewable energy continues to spur research in thin-film photovoltaics (PV), in particular those with chalcogenide semiconductor absorbers, which can combine high power conversion efficiencies (PCE) with efficient materials utilization. Solar cells based on cadmium telluride (CdTe) have achieved PCEs up to 20.4% and are produced at gigawatt-per-year (GW/yr) levels,[1] while PV cells based on copper (indium, gallium) (diselenide, disulfide) (CIGS) reach up to 20.9% PCE and are expected to enter GW/yr-level production in the near future.[2]

Materials utilization is becoming increasingly efficient in PV manufacturing, and as a result capital equipment comprises an ever larger fraction of module manufacturing costs.[3,4] Streamlined and high-throughput deposition systems are more easily realized when the physics of materials deposition works in one's favour. CdTe is a prominent example because the nearly equivalent vapour pressures of Cd and Te facilitate congruent evaporation, assisting feedstock purification to suppress deleterious second-phase particles and point defects. In general, the processing of binary systems is likely to be simpler compared to quaternary compounds including CIGS and Cu_2ZnSnS_4 (CZTS).

In this publication, we extend these principles to demonstrate the potential of tin sulfide (SnS) – a binary system and candidate replacement for CdTe. SnS has attracted interest as a PV absorber material due to its potential for large-scale, cost-effective and environmentally friendly power generation. Tin and sulfur are both non-toxic and abundant in nature. SnS benefits from favourable PV properties including a high optical absorption coefficient in the visible ($\geq 10^4$ cm^{-1}),[5–8] majority-carrier Hall mobility as high as 100 cm^2/Vs or higher,[5,9] and tunable majority-carrier density in the range of 10^{15} to 10^{18} cm^{-3}.[5,9]

During the past two years, thin-film solar cells based on SnS have shown substantial progress, improving from 1.3% to 4.36% certified efficiency.[5,10–14] So far, however, PV devices using thermally evaporated (TE) SnS have demonstrated low efficiencies. To date, the highest reported PCE for TE SnS solar cells is 1.6%, with a small device area of 0.01 cm^2.[10] The current SnS-based champion cell is processed using atomic layer deposition (ALD), achieving a certified PCE up to 4.36%.[14] Although highly valuable as an R&D tool, ALD is a rather slow and thus expensive fabrication method for growing films on the order of 1 µm thick, posing a challenge to industrial scale-up. Hence, there is a need to transfer learnings from ALD to higher-throughput manufacturing techniques without compromising quality.

We first demonstrate the ease of phase purification of commercial SnS powder by comparing the X-ray diffraction (XRD) patterns of as-purchased powder, post-annealed powder, and an evaporated thin film (**Figure 1**a). The purchased SnS powder (Alfa Aesar, batch # Lot K17U030) is nominally 99.5% pure Sn and S, i.e., not distinguishing between SnS and the phase impurities Sn_2S_3 and SnS_2. In the XRD pattern of the purchased powder we detect significant quantities of the sulfur-rich phases Sn_2S_3 (55% by weight) and SnS_2 (2%) in addition to the desired SnS phase (43%) (Figure 1a, black line). We anneal this precursor powder in a dedicated tube furnace under vacuum (approximately 15 mTorr) at 500 °C for 60 minutes to eliminate high vapour pressure contaminants and to achieve phase purity (Figure 1a, red line). The annealed SnS powder is then transferred into the deposition chamber for SnS film growth by congruent evaporation (Figure 1a, dark yellow line). Our XRD data indicate a substantial improvement in phase purity upon annealing the as-purchased powder. We see no peaks from the Sn_2S_3 or SnS_2 phases for the annealed powder, and the sensitivity of our measurement puts an upper limit of 0.2% on Sn_2S_3 phase fraction. The schematics on the right (Figure 1b through 1d) illustrate the different SnS feedstock conditions in line with the XRD spectra. Without treatment of the as-purchased powder, thermal evaporation of powder with sulfur-rich phase impurities would also yield a sulfur-rich SnS film.

We demonstrate the congruent evaporation process by comparing our deposition rates as a function of source temperature (T) to the published equilibrium pressure of SnS(g) over SnS(s). We calculate an equivalent SnS(g) vapour pressure from measured deposition rates using the Langmuir equation and assuming that the coefficient of evaporation $\alpha_e = 1$.[15] The agreement between our data and published equilibrium pressures of SnS(g) over SnS(s) shown in **Figure 2** demonstrates deposition by congruent evaporation. The systematic difference between our data and the equilibrium SnS(g) vapour pressure

Dr. V. Steinmann, Dr. R. Jaramillo, K. Hartman, R. Chakraborty, R. E. Brandt, J. R. Poindexter, Dr. Y. S. Lee, A. Polizzotti, Prof. T. Buonassisi
Massachusetts Institute of Technology
77 Massachusetts Avenue, Cambridge, MA 02139, USA
E-mail: vsteinma@mit.edu
L. Sun, H. H. Park, Prof. R. G. Gordon
Harvard University
Cambridge, MA 02138, USA

DOI: 10.1002/adma.201402219

© 2014 WILEY-VCH Verlag GmbH & Co. KGaA, Weinheim

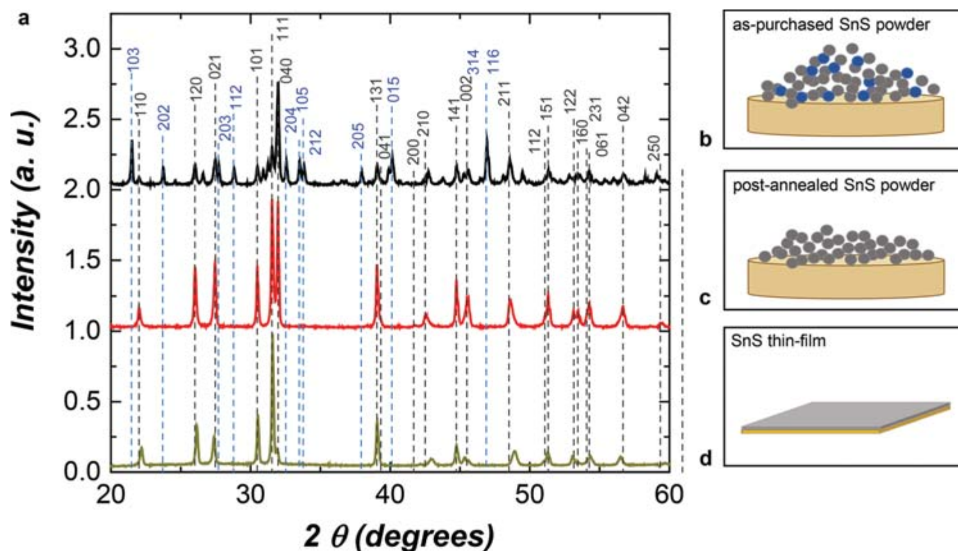

Figure 1. Natural purification of SnS feedstock. a XRD data of SnS powder and thin-films. We observe natural phase purification of the SnS powder by comparing the XRD of as-purchased SnS powder supplied by Alfa Aesar, batch # Lot K17U030 (black line) to the once post-annealed powder at 500 °C for 60 minutes (red line) and to a thermally evaporated SnS thin-film (dark yellow line). Note that the count rate for the SnS thin-film XRD (dark yellow line) is 3.75 times higher than for the SnS powder XRD (black and red lines). The vertical grey dashed lines indicate the peaks for the SnS phase and the blue dashed lines show select peaks for the sulfur-rich Sn_2S_3 phase; for clarity we only label those Sn_2S_3 peaks that appear strongly in our data for the as-purchased powder. The images on the right schematically show: b the as-purchased SnS powder with the blue particles representing sulfur-rich impurities and the grey particles representing the SnS phase, c the phase-pure, post-annealed SnS powder and d the phase-pure SnS thin-film.

suggests that $\alpha_e < 1$ for SnS; an excellent match is found using $\alpha_e = 0.34$ (red data points), consistent with the range observed for other binary compounds.[15]

In previous work, we demonstrated high performing SnS solar cells processed by ALD and pulsed chemical vapour deposition (p-CVD)[12–14] yielding a latest certified record device efficiency of 4.36% for an ALD-grown film.[14] SnS films deposited by either atomic layer deposition (ALD) or p-CVD result in densely packed, columnar layers with low surface roughness, favourable for solar cell fabrication.[6,12] However, typical ALD deposition rates are ~0.04 Å/s, making the device fabrication process time-consuming and thus expensive for potential industrial scale-up. In contrast, thermal evaporation of SnS is a much faster and therefore less expensive processing method.[22]

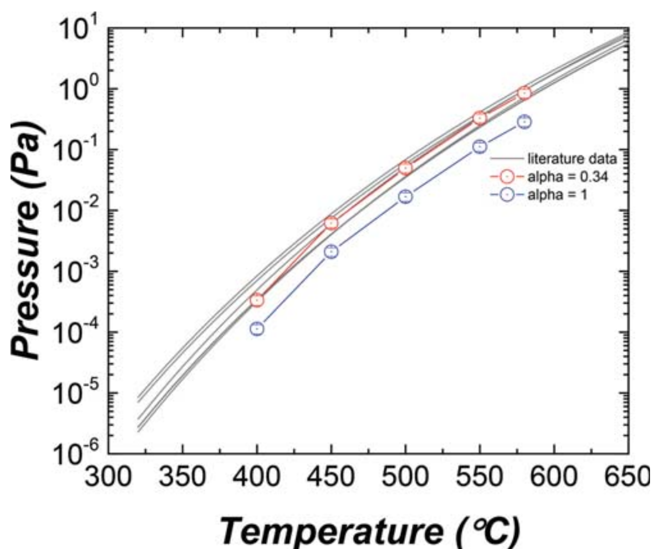

Figure 2. Equilibrium vapour pressure vs. source temperature demonstrating congruent evaporation. Solid lines are fits of the experimental vapour pressure of SnS(g) over SnS(s) from the literature.[16–21] Symbols and associated lines indicate our vapour pressure estimates based on measured deposition rates. The blue and red symbols show the vapour pressure estimated using $\alpha_e = 1$ and $= 0.34$, respectively.

Here we combine best practices in SnS-based device fabrication with thermal evaporation of SnS absorber layers. In essence, we demonstrate a manufacturing process similar to that used commercially for CdTe, but with Earth-abundant tin sulfide. We use SnS growth rates of 1 Å/s, 25 times faster than ALD. In principle, even higher deposition rates are possible by thermal evaporation. Preliminary results indicate an increase in SnS film porosity and surface roughness at very high deposition rates (~50 Å/s). We borrow the previously developed device stack for ALD grown devices,[14] yielding a PCE of 3.88% on 0.25 cm^2 device area. Our device layout and a schematic of the device stack are shown in **Figure 3**. Each substrate of 2.54 cm × 2.54 cm in size contains twelve nominally identical solar cells (see Figure 3a). The device stack is comprised of an oxidized Si wafer substrate, a Mo back contact, a two-layer Zn(O,S)/ZnO *n*-type buffer layer, indium tin oxide (ITO) as the transparent electrode, and Ag metallization (see Figure 3b).

For the solar cells reported here, we use SnS powder purchased from Sigma Aldrich (≥99.99%) and we apply the same purification procedure described above. We use 1200 ± 30 nm thick SnS films for the absorber layer. The large absorption coefficient of SnS ($\geq 10^4$ cm^{-1})[5–8] means that absorber layers less than 500 nm thick are sufficient to absorb much of the incident sunlight. For example, a 250 nm thick film will absorb 69% of

© 2014 WILEY-VCH Verlag GmbH & Co. KGaA, Weinheim
Adv. Mater. **2014**,
DOI: 10.1002/adma.201402219

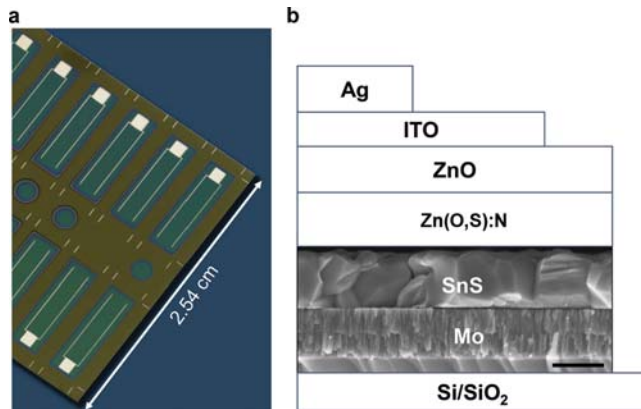

Figure 3. SnS thin-film solar cell. **a** A full-colour scan of an actual sample, showing the layout comprising 12 devices (each 0.25 cm^2 in area) on a 2.54×2.54 cm^2 Si/SiO_2 substrate. **b** schematically shows the device stack in profile. The layers are not drawn to scale. The cross-sectional SEM image depicts the Mo contact and the SnS absorber layer in the device stack; the scale bar indicates 500 nm. This SnS film was deposited and annealed following the same procedure as for our full solar cell devices, but the Mo and SnS thicknesses are different than those in our devices.

the AM1.5 solar resource above the 1.1 eV bandgap, yielding a maximum short-circuit current density (J_{SC}) of 30 mA cm^{-2}. However, we found that devices made with films less than 500 nm thickness had poor reproducibility due to shunting.

After deposition, the SnS films are annealed at 400 °C in a 4% H_2S (96% N_2) atmosphere at 28 Torr for 60 minutes to promote grain growth. After the annealing step and before buffer layer deposition, we modify the SnS surface with a very thin layer of SnO_2 (<1 nm). The SnO_2 layer was found to improve the SnS/Zn(O,S) interface, leading to higher V_{OC} values.[14] Detailed investigations of the TE SnS/Zn(O,S) interface are ongoing. Independent studies on the band alignment of SnS and different *n*-type buffers and its effect on the solar cell performance have been published.[23,24]

Figure 4 shows the solar cell characteristics for a representative TE SnS device with an PCE of 3.5% as measured in our laboratory. Figure 4a shows representative *J–V* data in the dark (dashed line) and under 1 Sun illumination (solid line). In Figure 4b, we present the EQE spectra of a typical TE SnS solar cell with a 0.3 Suns white light bias (solid red line) and without (dashed red line). The similarity of these spectra suggests that our devices respond linearly to injection level.

Our measured J_{SC} represents only 46% of the available above-bandgap light (λ < 1100 nm). In Figure 4b, we perform a current loss analysis for the wavelength range of 270 – 1100 nm, based on separately measured optical data for each layer in the device stack (see Supplemental Materials for details). 14% of the light (6.5 mA cm^{-2}) is lost due to reflection and shading, as determined by optical reflectance measurements on the same sample. We use the measured absorption coefficient of our bare ITO films and the Beer-Lambert law to calculate that 9% (4.1 mA cm^{-2}) of the light is lost due to absorption in the window layer (*i.e.*, Zn(O,S)/ZnO/ITO). Similarly, we use the measured absorption coefficient of our bare SnS films and the Beer-Lambert law to calculate that 12% (5.3 mA cm^{-2}) of the light passes through the SnS absorber layer due to the low absorption coefficient of SnS at long wavelengths. This light is presumably absorbed by the Mo back contact (we do not consider back-surface reflection). Finally, 19% (8.4 mA cm^{-2}) of the incident light is absorbed in the SnS layer but does not result in photocurrent, presumably because the carriers are lost to recombination. As expected, most of this recombination loss is at long wavelengths. Although this model is simple and does not include multiple optical path-lengths through the cell, it matches the measured EQE curve well at short wavelengths (where we expect excellent charge collection) and clarifies the necessary steps for further improving device efficiency. Through careful design of an anti-reflection-coating (ARC) and metallization pattern, we may realistically expect to reduce reflection and shading losses from 14% to below 5%, yielding a J_{SC} boost of >2.0 mA cm^{-2} (after considering losses in the stack). The biggest current loss mechanism is the 19% of the incident light that is absorbed in the SnS layer but not collected as current. To reduce these recombination losses, we need to improve the minority carrier diffusion length in the SnS bulk and passivate interfaces. For example, a twofold reduction in recombination loss would yield a J_{SC} boost of 4.2 mA cm^{-2}. In addition to these current-boosting steps, the fill factor (FF) could be improved by improving our series and shunt resistances. For the device shown in Figures 4 the series resistance (R_s) is sufficiently low (0.66 Ω cm^2) but the shunt resistance (R_{sh}) is rather low at

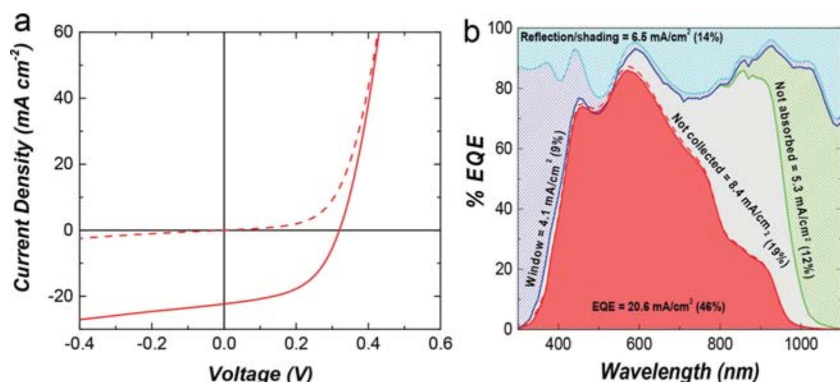

Figure 4. **a** Test results for a typical 0.25 cm^2 SnS solar cell. The device stack is: Si/SiO_2/Mo (720 nm)/SnS (1200 nm)/Zn(O,S) (30 nm)/ZnO (10 nm)/ITO (200 nm)/Ag (500 nm). a shows the *J–V* curves under 100 mW cm^{-2} (AM 1.5 conditions) illumination (solid line) and in the dark (dashed line). **b** shows the EQE spectra of a typical TE SnS solar cell with light bias of 0.3 Suns (solid red line) and without (dashed red line). We also use measured optical data to separate the different current loss mechanisms for above-bandgap light (λ < 1100 nm). Current densities are calculated by integrating the wavelength-resolved loss mechanisms over the AM 1.5 spectrum. 6.5 mA cm^{-2} is lost due to reflection and shading (light blue line), 4.1 mA cm^{-2} is absorbed in the window layer (blue line), 5.3 mA cm^{-2} passes through the SnS due to the low absorption coefficient at long wavelengths (green line), and 8.4 mA cm^{-2} is absorbed but not collected at the junction. The percentages in parentheses show the fraction of the total AM 1.5 spectrum that is lost or collected; e.g., 6.5 mA cm^{-2} is 15% of the total λ < 1100 nm flux of 43.3 mA cm^{-2}.

© 2014 WILEY-VCH Verlag GmbH & Co. KGaA, Weinheim

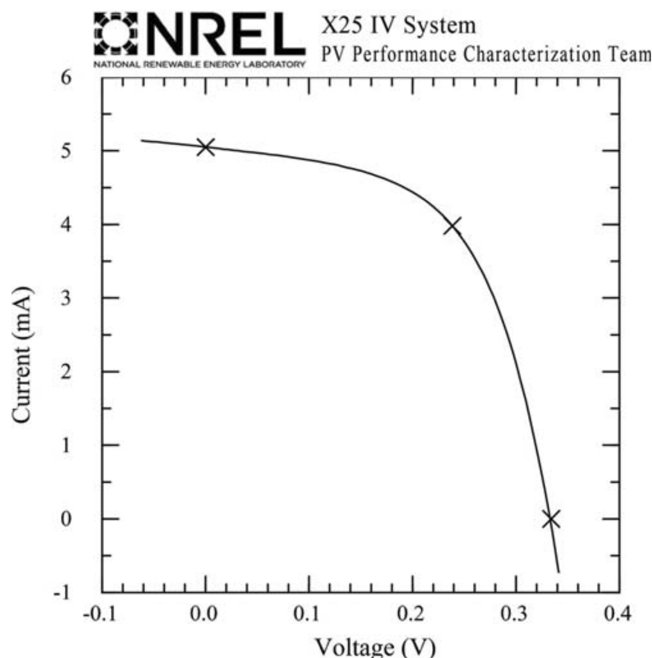

Figure 5. *I*–*V* characteristics of NREL-certified TE SnS solar cell: V_{OC} = 334.1 mV, J_{SC} = 20.645 mA/cm^2, FF = 56.28%, PCE = 3.88%. The device stack is: Si/SiO_2/Mo (720 nm)/SnS (1200 nm)/Zn(O,S) (30 nm)/ZnO (10 nm)/ITO (200 nm)/Ag (500 nm).

74 Ω cm^2. If the shunt resistance could be improved to 1000 Ω cm^2, perhaps by preventing pinholes through the SnS film and current pathways around the edge of the device, we calculate that the FF would improve by approximately 15% relative. Individually, each of the improvements outlined here represents a rather straightforward continuation of our work on SnS solar cells. Added together they imply that the PCE could improve by 46% (relative), yielding a 5.6% efficient SnS solar cell in the near future. To ultimately reach PCEs in the double digits, further optimization of the SnS bulk as well as the device stack will be needed.

Our process yields good solar cell reproducibility with small device-to-device variation. The solar cell characteristics (average ± standard deviation) measured at MIT from ten individual devices are: V_{OC} = 317 ± 9 mV, J_{SC} = 22.6 ± 0.8 mA/cm^2, FF = 54 ± 4%, PCE = 3.5 ± 0.4%. **Figure 5** reveals the NREL certified *I*–*V* data for our best device: V_{OC} = 334.1 mV, J_{SC} = 20.645 mA/cm^2, FF = 56.28%, PCE = 3.88%. The certified V_{OC} and FF are higher than the average of our in-house measurement by 5% and 12%, respectively, and the certified J_{SC} is 10% lower. These measurement differences could be partly due to a higher operating temperature (40 ± 5 °C) for *J*–*V* measurements at MIT compared to room temperature (24.7 ± 0.5 °C) measurements at NREL. At NREL, the solar cell was measured again after 10 minute light soaking at the maximum power point (P_{max}) followed by a 5 minute cool down. The certified PCE after light soaking was 3.86%.

In summary, we demonstrate the potential of congruent evaporation of SnS for thin-film solar cell applications. Thermal evaporation can enable relatively fast growth rates (here we compare to ALD) and potential industrial scale-up. The commercially available SnS powder is purified by pre-annealing in a separate furnace and by the process of congruent evaporation during film growth. We fabricate and optimize TE SnS solar cells, achieving an NREL-certified PCE of 3.88% for a 0.25 cm^2 device. By quantifying J_{SC} loss mechanisms, we suggest that more efficient charge collection, the addition of an anti-reflection-coating, and an improved top metal contact design could bring J_{SC} above 28.8 mA cm^{-2}. Combined with a higher shunt resistance up to 1000 Ω cm^2, these improvements could result in a PCE up to 5.6%. The device efficiency may be further improved by optimizing the annealing conditions and the buffer layer composition, which were fixed for this study.[24,25]

Experimental Section

The effective SnS(g) vapour pressure in Figure 2 was calculated from measured deposition rates on an unheated quartz crystal monitor (QCM) using the Langumir equation.[15] We assume that SnS sticks to the QCM with an adhesion coefficient of unity. The SnS source is a crucible with an orifice area of 0.785 cm^2, and the QCM is located 10.1 cm directly above the orifice. The SnS(g) flux from the source is calculated under the assumption of a cosine distribution from a point source.

All devices were fabricated on commercial Si/SiO_2 wafers. For this study we chose Si/SiO_2 wafers over conventional glass substrates to ensure well controlled experiments without the influence of sodium (Na) or other common glass additives or surface contaminants. In addition, we found the cleaning of Si/SiO_2 wafers to be straightforward and reproducible in contrast to our experience with commerically purchased glass substrates. The wafers were cleaned in a hot solvent bath prior to the Mo deposition. Mo was sputtered in two layers: an adhesive layer that was grown at 10 mTorr, and a conductive layer that was grown at 2 mTorr. The total Mo films were 720 nm thick with a typical sheet resistance of 0.85 Ω/sq. SnS was deposited in a thermal evaporator in the Langmuir configuration under high-vacuum conditions (10^{-7} – 10^{-8} Torr). During deposition the substrate was held at 240 ± 30 °C. Substrate rotation was used to guarantee uniform coverage. The substrate was kept 10 cm above the crucible orifice. The SnS film was annealed for 60 minutes in 4% H_2S (96% N_2) at 400 °C, with a total pressure of 28 ± 1 Torr. The thin SnO_2 layer was grown by exposure to ambient air for 24 hours at room temperature. Zn(O,S) (30 nm) and ZnO (10 nm) were grown at 120 °C by ALD. ITO (200 nm) was sputtered at low power (50 W) from a commercial ITO target with 20/0.2 sccm Ar/O_2 gas flow and a total pressure of 3 mTorr. ITO films were 220 nm thick with a typical sheet resistance of 40 Ω/sq. Ag fingers and contact pads were used for metallization.

J–*V* characteristics and EQE were measured at the MIT PVLab and at NREL by the PV certification team. At MIT, the *J*–*V* data was taken with a Keithley 2400 sourcemeter. The standard 100 mW cm^{-2} (1 Sun) illumination was generated by a Newport Oriel 91194 solar simulator with a 1300 W Xe-lamp using an AM1.5G filter, and a Newport Oriel 68951 flux controller calibrated by an NREL-certified Si reference cell equipped with a BK-7 window. EQE measurements were performed with a PV Measurements Model QEX7 tool at room temperature with and without light bias. The light bias was approximately 0.3 Suns.

The EQE losses were calculated by adding the reflectance of the entire device stack and the absorptance of individual layers. The device reflectance was measured directly. The absorption coefficients of our SnS, Zn(O,S), ZnO, and ITO materials were calculated from transmission and reflection measurements taken on bare films using a Perkin-Elmer Lambda 950 UV-Vis spectrophotometer, with 150 mm integrating sphere. The absorption of these layers in the device was then calculated from the absorption coefficients and the known layer thicknesses, assuming a single optical pass and Beer-Lambert exponential extinction. Of the light that makes it through this window layer (*i.e.*, Zn(O,S)/ZnO/

© 2014 WILEY-VCH Verlag GmbH & Co. KGaA, Weinheim
Adv. Mater. **2014**,
DOI: 10.1002/adma.201402219

ITO), the absorptance in the SnS was similarly calculated by assuming a single optical pass and exponential Beer-Lambert absorption. The total photocurrent (measured in % of AM1.5 spectrum for $\lambda < 1100$ nm or in mA cm^{-2}) lost in each layer was calculated using the fraction of lost photons from this EQE analysis and the AM1.5 spectrum.

The morphology of SnS films was imaged by field-emission SEM (FESEM, Zeiss, Ultra-55). The crystal structure and texture of the films were analysed by x-ray diffraction (XRD, Rigaku SmartLab) with Cu $K\alpha$ radiation using a θ-2θ scan.

VS led the experimental planning. VS, RJ, RC, KH and REB wrote the paper. VS and RJ led the device fabrication, characterization and data analysis. KH led the powder and thin-film annealing studies and XRD analysis. RC led the congruent evaporation study on SnS. REB was involved in the device characterization and data analysis. JRP took the EQE data. YSL and LS were involved in the device fabrication. AP assisted with the H_2S annealing studies. HHP was involved in the buffer layer development leading to the champion device. RGG and TB led the overall project as the PIs of the collaborating labs at Harvard and MIT, including assisting the team with data interpretation, structuring, and presentation.

Supporting Information

Supporting Information is available from the Wiley Online Library or from the author.

Acknowledgements

The authors would like to thank Paul Ciszek and Keith Emery from the National Institute for Renewable Energy (NREL) for certified *J–V* measurements. The authors are thankful to Mariela Lizet Castillo for helping with substrate preparation, Dr. Jasmin Hofstetter and Dr. Niall Mangan for fruitful scientific discussions and Felice Frankel for graphic designs. This work is supported by the U.S. Department of Energy through the SunShot Initiative under contract DE-EE0005329, and by Robert Bosch LLC through the Bosch Energy Research Network under grant 02.20.MC11. V. Steinmann, R. Jaramillo, K. Hartman, and R. E. Brandt acknowledge the support of, the Alexander von Humboldt foundation, a DOE EERE Postdoctoral Research Award, an Intel PhD Fellowship, and an NSF GRFP Fellowship respectively. This work made use of the Center for Materials Science and Engineering at MIT which is supported by the National Science Foundation (NSF) under award DMR-08–19762, and the Center for Nanoscale Systems at Harvard University which is supported by NSF under award ECS-0335765.

Received: May 16, 2014
Revised: July 3, 2014
Published online:

[1] http://www.firstsolar.com. First Solar, **2014**, *Press Release February 25th*.
[2] http://www.solar-frontier.com. Solar Frontier, **2014**, *Press Release April 2nd*.
[3] M. Woodhouse, A. Goodrich, R. Margolis, T. L. James, M. Lokanc, R. Eggert, *IEEE J. Photovoltaics* **2012**, PP. 1.
[4] M. Woodhouse, A. Goodrich, R. Margolis, T. L. James, R. Dhere, T. Gessert, T. Barnes, R. Eggert, D. Albin, *Sol. Energy Mater. Sol. Cells* **2013**, *115*, 199.
[5] K. T. Ramakrishna Reddy, N. Koteswara Reddy, R. W. Miles, *Sol. Energy Mater. Sol. Cells* **2006**, *90*, 3041.
[6] P. Sinsermsuksakul, J. Heo, W. Noh, A. S. Hock, R. G. Gordon, *Adv. Energy Mater.* **2011**, *1*, 1116.
[7] A. Tanuševski, *Semiconductor Science and Technology* **2003**, *18*, 501.
[8] K. Hartman, J. L. Johnson, M. I. Bertoni, D. Recht, M. J. Aziz, M. A. Scarpulla, T. Buonassisi, *Thin Solid Films* **2011**, *519*, 7421.
[9] H. Noguchi, A. Setiyadi, H. Tanamura, T. Nagatomo, O. Omoto, *Sol. Energy Mater. Sol. Cells* **1994**, *35*, 325.
[10] A. Schneikart, H.-J. Schimper, A. Klein, W. Jaegermann, *J. Phys. D. Appl. Phys.* **2013**, *46*, 305109.
[11] T. Ikuno, R. Suzuki, K. Kitazumi, N. Takahashi, N. Kato, K. Higuchi, *Appl. Phys. Lett.* **2013**, *102*, 193901.
[12] P. Sinsermsuksakul, K. Hartman, S. B. Kim, J. Heo, L. Sun, H. Park, R. Chakraborty, T. Buonassisi, R. G. Gordon, *Appl. Phys. Lett.* **2013**, *102*, 053901.
[13] H. H. Park, R. Heasley, L. Sun, V. Steinmann, R. Jaramillo, K. Hartman, R. Chakraborty, P. Sinsermsuksakul, D. Chua, T. Buonassisi, R. G. Gordon, *Prog. Photovoltaics* **2014**, DOI: 10.1002/pip.2504.
[14] P. Sinsermsuksakul, L. Sun, S. W. Lee, H. H. Park, S. B. Kim, C. Yang, R. G. Gordon, *Adv. Energy Mater.* **2014**, DOI: 10.1002/aenm.201400496.
[15] G. M. Pound, *J. Phys. Chem. Ref. Data* **1972**, *1*, 135.
[16] V. Piacente, S. Foglia, P. Scardala, *J. Alloys Compd.* **1991**, *177*, 17.
[17] R. Colin, J. Drowart, *J. Chem. Phys.* **1962**, *37*, 1120.
[18] W. H. St. Clair, B. K. Shibler, I. S. Solet, *U.S. Bur. Mines Rept. Invest.* **1954**, 5095.
[19] D. N. Klushin, V. Y. Chernykh, *Zhur. Neorg. Khim.* **1960**, *5*, 1409.
[20] H. Rau, *Ber. Bunsenges, Physik. Chem.* **1967**, *71*, 716.
[21] A. W. Richards, *Trans. Faraday Soc.* **1955**, *51*, 1193.
[22] O. E. Ogah, G. Zoppi, I. Forbes, R. W. Miles, *Thin Solid Films* **2009**, *517*, 2485.
[23] L. Burton, A. Walsh, *Appl. Phys. Lett.* **2013**, *102*, 132111.
[24] L. Sun, R. Haight, P. Sinsermsuksakul, S. B. Kim, H. H. Park, R. G. Gordon, *Appl. Phys. Lett.* **2013**, *103*, 181904.
[25] H. H. Park, R. Heasley, R. G. Gordon, *Appl. Phys. Lett.* **2013**, *102*, 132110.

© 2014 WILEY-VCH Verlag GmbH & Co. KGaA, Weinheim